Agonist Binding to the *Torpedo* Acetylcholine Receptor. 2. Complexities Revealed by Association Kinetics[†]

Susan M. J. Dunn*[,‡] and Michael A. Raftery[§]

Department of Pharmacology and Division of Neuroscience, University of Alberta, Edmonton, Alberta, Canada T6G 2H7, and Department of Biochemistry, University of Minnesota, St. Paul, Minnesota 55108, and Department of Pharmacology, University of Minnesota School of Medicine, Minneapolis, MN 55455

Received June 21, 1996; Revised Manuscript Received January 17, 1997[⊗]

ABSTRACT: The binding of suberyldicholine to membrane-bound *Torpedo* acetylcholine receptor has been monitored by fluorescence changes of covalently bound 5-iodoacetamidosalicylic acid (IAS). At equilibrium, suberyldicholine binds to two high-affinity binding sites ($K_d \approx 20$ nM). Kinetic experiments reveal that there is rapid formation of an initial complex ($K_d \approx 2$ μM) which undergoes sequential fast ($k_{app} \approx 1$ s^{-1}) and slow ($k_{app} \approx 0.05$ s^{-1}) conformational changes. These kinetics differ from those reported for other agonists [Blanchard, S. G., Dunn, S. M. J., & Raftery, M. A. (1982) *Biochemistry 24*, 6258−6264] in that, for suberyldicholine, there is no evidence for a second pathway involving the binding of an additional agonist molecule. These results, considered together with the observed dissociation kinetics (accompanying manuscript), suggest that each high-affinity site for acetylcholine is made up of two subsites, which suberyldicholine is able to bridge, thus occluding the binding of a second ligand. The kinetic mechanism for acetylcholine binding has been re-examined to accommodate the complexities of the [^{3}H]-acetylcholine dissociation kinetics and the observation that, at equilibrium, no more than two occupied binding sites are detected [accompanying manuscript: Dunn, S. M. J., & Raftery, M. A. (1997) *Biochemistry 36*, 3846−3853]. It is suggested that, for each acetylcholine binding site, a second ligand is able to bind but that the ternary complex is transient since one of the two bound ligands again dissociates in the formation of the equilibrium mono-liganded complex. To further probe the physical nature of the two subsites, the binding of a series of bis-quaternary suberyldicholine analogues, $(CH_3)_3N^+CH_2CH_2OCO$-$(CH_2)_n$-$COOCH_2CH_2N^+(CH_3)_3$, to IAS-labeled receptor preparations has been examined. Analogues in which $n < 5$ behave like acetylcholine, i.e., a second ligand binding pathway is observed, but longer ligands ($n = 5-10$) act like suberyldicholine and may be long enough to cross-link the sites.

The abundance of the nicotinic acetylcholine receptor (nAcChR)[1] in *Torpedo* electric organ provides a unique opportunity for detailed studies of the mechanisms by which agonists bind and induce the protein conformational changes that result in channel activation and receptor desensitization [reviewed by Stroud et al. (1990), Changeux (1995), and Karlin and Akabas (1995)]. Similar studies of the homologous $GABA_A$, glycine, and 5-HT_3 receptors cannot approach the same level of sophistication because of the very low natural abundance of these proteins and, often, the confounding influence of receptor heterogeneity [reviewed by Betz (1990), Dunn et al. (1994), and Sieghart (1995)]. Thus the nAcChR is often used as a model for this receptor family, with the reasonable expectation that all members share common functional properties [reviewed by Barnard (1992) and Hollenberg (1991)]. However, the nAcChR receptor is a large, complex membrane-bound protein, being a pentamer of homologous subunits [$\alpha_2\beta\gamma\delta$; see Raftery et al. (1980) and Noda et al. (1983)] assembled around a central cation channel. This, in addition to the present lack of detailed three-dimensional structural information, makes mechanistic studies and their interpretation much more difficult than similar studies of, for example, relatively small soluble enzymes. Undoubtedly, agonist binding to the nAcChR is complex as is illustrated by the substantial differences in the kinetic behavior that are observed using different approaches, e.g., radiolabeled ligands (Boyd & Cohen, 1980), fluorescent cholinergic ligands (Prinz & Maelicke, 1983; 1992; Heidmann & Changeux, 1979, 1980) and covalent (Dunn et al., 1980; Dunn & Raftery, 1982, 1993) or reversibly bound (Grünhagen et al., 1977; Quast et al., 1979) extrinsic probes. Although a variety of complex mechanisms have been proposed [see Ochoa et al. (1989) and Prinz (1988)], none can accommodate all of the available experimental data. As with all complicated systems, it is thus likely that current views about the receptor mechanism are overly simplistic.

Equilibrium binding studies using radiolabeled agonists have shown that each nAcChR carries two high-affinity binding sites. In many reports, though not all [see Changeux et al. 1(984) and Prinz and Maelicke (1993)], these sites have been shown to be independent [e.g., Dunn et al. (1980) and Blanchard et al. (1982)] or only weakly cooperative [re-

[†] This work was supported by the Medical Research Council of Canada (S.M.J.D.) and by NIDA Program Project Grant DA08131 (M.A.R.). S.M.J.D. is an MRC Scientist.

* Author to whom correspondence should be addressed at Department of Pharmacology, 9−70 Medical Sciences Building, University of Alberta, Edmonton, Alberta, Canada T6G 2H7. Tel: (403) 492-3414. FAX: (403) 492-4325. E-mail: Susan.Dunn@UAlberta.ca.

[‡] University of Alberta.

[§] University of Minnesota.

[⊗] Abstract published in *Advance ACS Abstracts,* March 1, 1997.

[1] Abbreviations: AcCh, acetylcholine chloride; α-BuTx, α-bungarotoxin; Carb, carbamylcholine chloride; IAS, 5-iodoacetamidosalicylic acid; nAcChR, nicotinic acetylcholine receptor; SdCh, suberyldicholine diiodide.

S0006-2960(96)01504-8 CCC: $14.00

viewed by Taylor et al. (1983)]. Early affinity labeling experiments showed that these sites are associated with the α-subunits, since following reduction of a reactive disulfide bond near the sites, the α-subunits could be labeled with the affinity alkylating antagonist, [^{3}H]MBTA, or the agonist, [^{3}H]bromoacetylcholine (Damle & Karlin, 1978; Moore & Raftery, 1979; Wolosin et al., 1980). The reactive disulfide bond has since been shown to be formed by a pair of vicinal cysteines at positions 192 and 193 in the extracellular amino-terminal domain (Kao et al., 1984; Kao & Karlin, 1986; Mosckovitz & Gershoni, 1988; Kellaris & Ware, 1989). More recently, by looking at expression of subunit pairs (Blount & Merlie, 1989; Sine & Claudio, 1991), by photoaffinity labeling with agonists (Middleton & Cohen, 1991) and antagonists (Pederson & Cohen, 1990; Kreienkamp et al., 1992) and by affinity labeling (Dunn et al., 1993), evidence has been accumulating to suggest that these sites are not associated exclusively with the α-subunits, but rather may occur at the α−γ and α−δ subunit interfaces. In addition to labeling studies, site-directed mutagenesis has provided information about specific amino acid residues that may be involved in ligand recognition (Galzi et al., 1991; Tomaselli et al., 1991; O'Leary & White, 1992; Czajkowski et al., 1993; Sine, 1993; Sine et al., 1995) and this has led to models in which several protein loops in the α-subunits, and specific residues in the γ and δ subunits, contribute to the formation of each of the two high-affinity binding sites [reviewed by Changeux et al. (1992)].

In the accompanying manuscript, where we describe the kinetics of dissociation of [^{3}H]acetylcholine (AcCh) and [^{3}H]-suberyldicholine (SdCh), a further complexity in high-affinity binding was revealed. Micromolar concentrations of unlabeled agonists increased the dissociation rate of bound [^{3}H]-AcCh even when it originally saturated all of the high-affinity sites. This suggested the presence of an additional binding site, but, within the experimentally accessible concentration range of ligand (0−20 μM), this was not detected in equilibrium binding studies. It was therefore proposed that each high-affinity site for AcCh is made up by two subsites (A and B) which, at least over this concentration range, are mutually exclusive at equilibrium. With [^{3}H]AcCh originally occupying site A, the binding of an additional molecule to site B drastically reduces the affinity of site A for [^{3}H]AcCh and its dissociation is accelerated. Parallel studies of [^{3}H]-SdCh offered a possible clue as to the physical nature of these subsites. Since the dissociation of [^{3}H]SdCh was only marginally, if at all, affected by added unlabeled ligand, it was suggested that this large, flexible, bis-quaternary agonist $[CH_3)_3N^+CH_2CH_2COO(CH_2)_6OCOCH_2CH_2N^+(CH_3)_3]$ can either physically bridge the subsites or at least sterically inhibit site B so as to prevent a second ligand from binding.

In the present report we describe the kinetics of SdCh and AcCh binding to nAcChR-enriched membranes that have been covalently labeled with the environmentally-sensitive fluorescent probe, 5-iodoacetamidosalicylic acid (IAS). The fluorescence of IAS is sensitive to the binding of agonists and competitive antagonists to the high-affinity sites associated, at least in part, with the α-subunits (Dunn et al., 1980; Blanchard et al., 1982; Dunn & Raftery, 1993). It has previously been shown that the ligand-induced fluorescence enhancement is due specifically to IAS labeling of reduced disulfide Cys192-Cys193 close to the binding site (Dunn & Raftery, 1993). In other previous reports we have used a different fluorescent probe (IANBD) to measure binding of agonists to distinct low-affinity sites that may be involved in channel activation (Dunn & Raftery, 1982a,b, 1993; Dunn et al., 1983). It is emphasized that in the present report, as well as in the accompanying manuscript (Dunn & Raftery, 1997), we are looking *only* at the complexities of the high-affinity sites and not at low affinity agonist binding sites.

It is demonstrated that the kinetics of association of AcCh are more complex than those of SdCh and, as described for the dissociation kinetics (accompanying manuscript), may be explained by the presence of an additional binding site that can be occupied transiently in the association reaction. SdCh, being a large flexible ligand, is again depicted as being able to cross-link the binding sites. In further studies of the physical nature of the subsites, the binding of a series of bis-quaternary agonists with different physical dimensions has been examined. At a specific point in the series, the analogues change from mimicking AcCh in their association kinetics, i.e., with evidence for occupancy of an additional binding site, to acting like SdCh. This places physical restrictions on the distance between the two subsites.

EXPERIMENTAL PROCEDURES

Preparation of nAcChR-Enriched Membrane Fragments. nAcChR-enriched membranes were purified from electric organ of *Torpedo californica* and, after alkali-extraction, were assayed for protein and [^{125}I]-α-BuTx binding sites as described in the accompanying manuscript (Dunn & Raftery, 1997). All experiments were carried out at 25 °C using *Torpedo* Ringers (20 mM Hepes-Na^+, pH 7.4, 250 mM NaCl, 5 mM KCl, 2 mM $MgCl_2$, 4 mM $CaCl_2$, 0.02% NaN_3). Although the alkali treatment effectively destroys all acetylcholinesterase activity, as an added precaution, the membranes were pretreated with 50 μM Tetram prior to equilibrium fluorescence studies.

*Fluorescent Labeling of nAcChR-Enriched Membrane Fragments. Torpedo m*embranes were alkylated with the sulfhydryl-specific fluorescent probe, 5-iodoacetamidosalicylic acid (IAS) following mild reduction with 50 μM DTT and reaction with 250 μM IAS, as previously described (Dunn et al., 1980). IAS was synthesized as described by Haugland (1970).

Bis-Quaternary Ligands. Suberyldicholine (C8) and succinylcholine (C4) were purchased from Aldrich Chemical Company. The other bischoline esters used in these studies were synthesized from the corresponding acid chlorides [oxalyl chloride (C2), glutaryl chloride (C3), valeryl chloride (C5), adipyl chloride (C6), pimelyl chloride (C7), azelyl chloride (C9), decyl chloride (C10), and dodecyl chloride (C12), all from Aldrich]. The methods used have been described in detail (Mecklenborg & Orchin, 1958; Holmstedt & Whittaker, 1958; Sekull & Holland, 1961, 1963). Briefly, *N*,*N*-dimethylaminoethanol (Aldrich) was reacted with an acid chloride, and the resulting tertiary ammonium precipitate was washed extensively with fresh solvent. The product was then dissolved in carbonate−bicarbonate buffer at pH 10 (saturated with sodium chloride) and extracted into methylene chloride and dried over anhydrous magnesium sulfate. Quaternization was effected by reaction with excess methyl iodide. Structures were confirmed by ^{1}HNMR spectroscopy (Brucker).

Equilibrium Fluorescence Measurements. The binding of agonists to IAS-labeled membrane preparations was moni-

tored by the changes in IAS fluorescence measured by energy transfer from the receptor protein using excitation and emission wavelengths of 282 nm and 430 nm respectively (Dunn et al., 1980). A Perkin-Elmer MPF4 fluorimeter, with a magnetically stirred and thermostated cuvette holder, was used for all equilibrium experiments. Since IAS monitors high-affinity binding and there is significant depletion of added ligand due to binding, binding data were analyzed using InPlot Version 4.0 (GraphPad Software, San Diego, CA) and the following model (Dunn & Raftery, 1993):

$$Fl = F_{RL}[RL] = 0.5F_{RL}\{(L_0 + K_d + R_0) - \sqrt{[(L_0 + R_0 + K_d)^2 - 4R_0L_0]}\}$$

where Fl is the observed fluorescence (after subtraction of the fluorescence of IAS-labeled AcChR alone), L_0 is the added ligand concentration, R_0 is the concentration of binding sites and K_d and F_{RL} are the dissociation constant and fluorescence enhancement per unit concentration of RL complex, respectively. At saturation, the maximum observed fluorescence enhancement (F_{max}) is given by

$$F_{max} = F_{RL}[R_0]$$

Kinetic Measurements. The kinetics of binding of cholinergic agonists to IAS-labeled membranes were investigated using an Applied Photophysics Ltd. (Leatherhead, U.K.) SF17.MV stopped-flow fluorimeter with excitation at 282 nm and emission recorded using a Corning O-52 filter. A UV bandpass filter was placed in the excitation beam to reduce stray light. Data were collected by an Archimedes computer and analyzed using the Applied Photophysics software and a two-exponential model

$$F(t) = A_0 + A_1[\exp(-k_1t)] + A_2[\exp(-k_2t)] + k_0t$$

in which $F(t)$ is the fluorescence level at time t, A_0 is the equilibrium fluorescence level, k_0 is the slope of the base line (to correct for any nonspecific photolysis effects occurring on slow time scales), k_1 and k_2 are the apparent rate constants of the two processes, and A_1 and A_2 are the corresponding amplitudes. In many experiments (see below), a split time base was used to improve the resolution of biphasic kinetics. In the case of AcCh (and other agonists displaying similar kinetic behavior, see below), where the fluorescence enhancement has at least three components, data were collected over several different time scales. These were chosen so that no more than two phases were present to a significant extent in any one kinetic trace [see Dunn et al. (1980)]. These data were also fit by the two-exponential model above, in which the term k_0 was also used to correct for any linear component introduced by the initial phase of a subsequent slower reaction. For further analysis and mechanism fitting, parameters for any phase in which the time scale of the experiment was less than 2.5 or more than 25 times the half-time of that phase were excluded [see Dunn et al., (1980)]. These fitting procedures were used to obtain estimates of apparent rate constants (k_{app}) and the corresponding amplitudes for each kinetic phase and these parameters were subsequently used in model analysis.

Model Fitting and Simulations. Kinetic data were analyzed by multi-parameter nonlinear regression techniques (MicroMath SCIENTIST Version 2.03, Salt Lake City, UT)

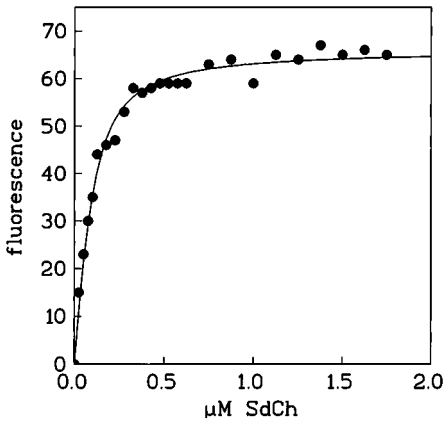

FIGURE 1: Equilibrium binding of SdCh to IAS-labeled *Torpedo* membranes (0.1 μM in [^{125}I]-αBuTx sites). Data were obtained in a fluorescence titration experiment and model fitting as described in the text gave the following best fit parameters: K_d = 26 nM, R_0 = 93 nM, and F_{max} = 66.6 (arbitrary units).

using explicit expressions given in the text, which were derived for the different mechanisms considered. Best fit parameters obtained for equilibrium constants, rate constants and amplitudes were then used to calculate the theoretical curves shown in the figures. In all kinetic mechanisms discussed, the isomerization equilibrium constants are defined as $K_i = k_{-i}/k_i$ where k_{-i} and k_i are the backward and forward rate constants, respectively.

RESULTS

Equilibrium Binding of SdCh. As described previously, the high-affinity binding of agonists to the nAcChR can be monitored by changes in the fluorescence of a fluorophore, IAS, covalently attached to the reduced disulfide at position 192/193 of the α-subunits. The data in Figure 1 show a typical fluorescence titration of IAS-labeled membranes by SdCh. The fluorescence enhancement is saturable, suggesting a homogeneous population of binding sites with a K_d of 26 nM, i.e., in good agreement with estimates obtained in direct binding studies using [^{3}H]SdCh (K_d = 15.9 ± 6.3 nM; see accompanying manuscript). In control experiments, it has been shown that IAS labeling does not affect the affinity or number of sites for [^{3}H]SdCh (data not shown).

Kinetics of SdCh Binding Monitored by IAS Fluorescence. Stopped-flow experiments have shown that the fluorescence enhancement occurring on SdCh binding to IAS-labeled membranes takes place in two phases which differ in rate by about 20-fold (Figure 2). The concentration dependencies of the apparent rates and amplitudes of these phases are shown in Figure 3. As described previously for the binding of other agonists to the nAcChR, the changes in fluorescence of bound IAS reflect conformational transition of the receptor−ligand complex and not the formation of the initial complex (Dunn et al., 1980; Blanchard et al., 1982; Dunn & Raftery, 1993). The faster rate has an approximately hyperbolic dependence on SdCh concentration, and the slower phase rate increases at low ligand concentrations and remains essentially constant at SdCh concentrations above 3 μM. These data are consistent with a model in which the initial binding of SdCh to the receptor is followed by two sequential conformational changes of the initial complex (Figure 4A). According to this scheme, if one makes the assumptions (a) that R and L equilibrate rapidly, i.e.,

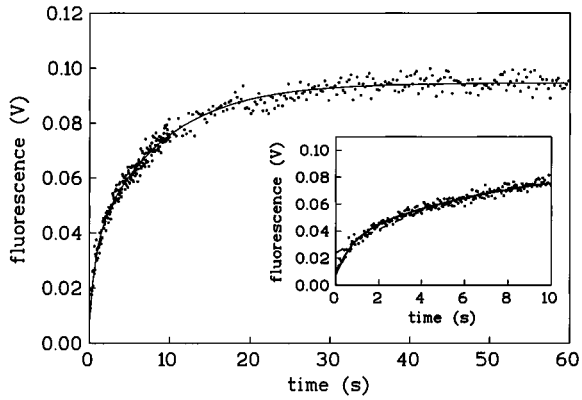

FIGURE 2: Kinetics of SdCh binding to IAS-labeled *Torpedo* membranes. Data show a representative stopped-flow trace of the binding of 3 μM SdCh to *Torpedo* membranes (approximately 0.25 μM in [^{125}I]-αBuTx sites). Data were recorded using a split time base with 200 points recorded from 0−10 s and 200 points recorded from 10−60 s. Solid line is best fit to a two-exponential equation with $A_1 = 27$ mV, $k_1 = 1.14$ s^{-1}, $A_2 = 61$ mV, $k_2 = 0.086$ s^{-1}. Inset shows expanded data on fast time scales and demonstrates clear deviation from a single-exponential model (dashed line).

formation of the initial RL complex is a rapid pre-equilibrium reaction, (b) that step 2 is considerably faster than step 3, and (c) that the each isomerization results in a change in the fluorescence intensity of the bound probe, then the two phases can be analyzed independently. The observed rate constants may be approximated by

$$k_{app}(\text{fast}) = \frac{k_2[L]}{K_1 + [L]} + k_{-2}$$

and

$$k_{app}(\text{slow}) = \frac{k_3[L]}{K_1K_2 + K_2[L] + [L]} + k_{-3}$$

At equilibrium, the total concentration of complex is the sum of the equilibrium concentrations of RL, R*L, and C_1, i.e.,

$$[\text{bound}] = [\text{RL}]_{eq} + [\text{R*L}]_{eq} + [\text{C}_1]_{eq}$$

$$= \frac{[R_0][L]}{[L] + K_d}$$

where

$$K_d = \frac{K_1K_2K_3}{1 + K_3(1 + K_2)}$$

In the kinetic studies, the total fluorescence enhancement observed (A_T) at the end of the reaction (i.e., at equilibrium) is the sum of the amplitudes of the fast (A_f) and slow (A_s) phases, which is also described by the relationship

$$A_T = Q_{R*L}[\text{R*L}]_{eq} + Q_{C_1}[\text{C}_1]_{eq}$$

where Q_{R*L} and Q_{C_1} are the fluorescence quantum yields of the R*L and C_1 complexes, respectively. As described above, the formation of the initial complex, RL, is not associated with any measurable change in fluorescence. Thus

$$A_T = \left[\frac{R_0[L]}{[L] + K_d}\right]\left[\frac{K_3Q_{R*L} + Q_{C_1}}{1 + K_3(1 + K_2)}\right]$$

Since step 2 is much faster than step 3, the amplitude of the fast phase may be estimated as

$$A_f \approx Q_{R*L}[\text{R*L}]_f \approx \frac{Q_{R*L}R_0[L]}{[L] + K_2([L]+K_1)}$$

where $[\text{R*L}]_f$ is the transient concentration of R*L that is formed in the initial fast phase, i.e., prior to rate-limiting conversion to C_1. The amplitude of the slow phase can then be approximated simply by

$$A_s \approx A_T - A_f$$

The slow phase includes the formation of C_1 from R*L formed in the initial fast phase plus the re-equilibration of RL, R*L, and C_1. This results in an apparent "overshoot"

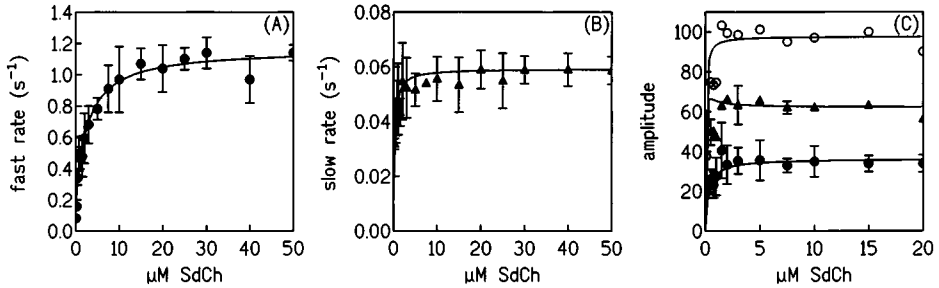

FIGURE 3: Dependence of kinetic parameters on SdCh concentration. Data were obtained in stopped-flow experiments as in Figure 2 and show concentration dependence of (A) the fast phase rate, (B) the slow phase rate and (C) corresponding fast (●), slow (▲) and total (○) amplitudes. Data were pooled from four independent titrations, with at least triplicate estimates of each parameter being made in each titration. Data are shown as the mean ± SD of all estimates. Solid lines are calculated from the best fit parameters to the model given in the text (Figure 4A) with the best fit parameters given in Table 1. Nonlinear regression techniques without constraint were first used to estimate values of K_1, k_2, and k_{-2} from the rates of the fast phase. These values and the corresponding value of K_2 were then fixed to obtain initial estimates of k_3 and k_{-3} from the concentration dependence of the apparent rate of the slow phase. All parameters were then allowed to vary in simultaneous analysis of the rate data for both phases. Estimates of the equilibrium constants were then fixed in analysis of the fast phase amplitude to give an estimated value for Q_{R*L} of 42.6. Using this value, the total amplitude and slow phase amplitude were then simultaneously analyzed giving an estimated Q_{C_1} of 62.8. There was a high level of consistency in the best fit parameters obtained for all phases and a simple iterative procedure rapidly converged on a consistent set of parameters.

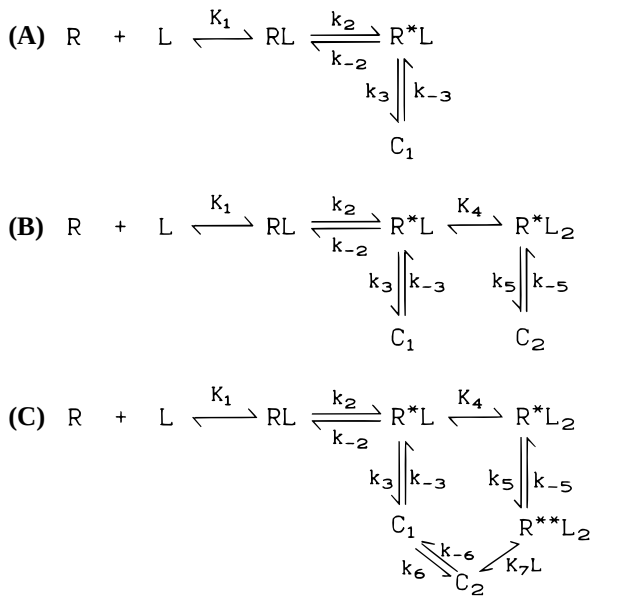

FIGURE 4: Kinetic schemes consistent with data for agonist binding to *Torpedo* membrane-bound nAcChR. In each case, R represents the initial conformation of only one of the two high-affinity sites of the nAcChR (see text), i.e., all schemes must be doubled to describe both high-affinity binding sites in the receptor. (A) Model used for analysing the kinetic data for SdCh binding (Figure 3). (B) Original model used to describe the AcCh binding kinetics [Blanchard et al., 1982; see also Quast et al. (1979), Dunn et al. (1980), and Dunn and Raftery (1993)]. (C) Expanded model to account for the AcCh binding kinetics and to include more recent experimental observations (see text and accompanying manuscript) that (i) di-liganded receptor, i.e., R^*L_2 and $R^{**}L_2$ do not exist in significantly measurable amounts at AcCh concentrations up to 20 μM and that (ii) micromolar concentrations of AcCh are able to accelerate the dissociation of [^{3}H]AcCh previously saturating the high-affinity sites.

Table 1: Parameters Obtained from Model Fitting of the SdCh Kinetic Data by Figure 4A and of AcCh Kinetic Data by Figures 4B and 4C

parameter	SdCh binding Figure 4A	AcCh binding Figure 4B	AcCh binding Figure 4C
K_1 (μM)	1.98	3.33	4.99
k_2 (s^{-1})	0.92	8.45	8.11
k_{-2} (s^{-1})	0.16	0.99	1.28
k_3 (s^{-1})	0.063	0.27	0.62
k_{-3} (s^{-1})	0.010	0.023	0.023
K_4 (μM)	–	3.51	74.2
k_5 (s^{-1})	–	1.69	2.67
k_{-5} (s^{-1})	–	0.53	0.15
K_6	–	–	2.79
K_7 (μM)	–	–	39.9
$K_1K_2K_3$ (μM)	0.055	0.033	0.029
K_4K_5/K_3 (μM)	–	12.9	112.4

in A_s (see Figure 3C) at ligand concentrations below saturation of R*L (due to the RL → R*L → C_1 pathway). The solid lines in Figure 3 are theoretical curves derived from fitting by this model and the best fit kinetic parameters are given in Table 1. The estimated value for the overall dissociation constant (K_d) calculated from the kinetic parameters (46 nM) is in reasonable agreement with that obtained from the equilibrium fluorescence titrations (Figure 1) and direct binding studies of [^{3}H]SdCh (accompanying manuscript). It should be noted that Figure 4A depicts binding to only one of the two high-affinity sites known to exist on each nAcChR (see introduction), i.e., the scheme should be doubled to represent the intact receptor.

SdCh and AcCh Display Differences in Their Association Kinetics. The mechanism for SdCh binding to IAS-labeled nAcChR (Figure 4A) differs in one major respect from the mechanism (Figure 4B) which was previously proposed to account for the kinetics of binding of other agonists monitored using either covalently bound IAS (Dunn et al., 1980; Blanchard et al., 1982; Dunn & Raftery, 1993) or reversibly bound ethidium (Quast et al., 1979). A dominant feature observed in the binding of the agonists previously studied, was a slow phase ($k_{app} = 0.02-0.12$ s^{-1}) which was obvious at low ligand concentrations but which was reduced in both rate and amplitude at higher concentrations (see below and, e.g., the Carb kinetics in Figure 7). Although many possible mechanisms were evaluated [see Quast et al., (1979)], this behavior was found to be consistent *only* with an asymmetric, branched mechanism involving the binding of an additional ligand (e.g. Figure 4B). According to Figure 4B, at low ligand concentrations, the slow pathway (step 3) toward C_1 is favored, but at higher ligand concentrations, an additional ligand binds to R*L and favors the reaction toward C_2. In the case of SdCh, although the slow phase has a similar rate to that observed for other agonists, there is no evidence for the binding of an additional ligand to R*L.

Correlation of Association Kinetics Revealed by IAS Fluorescence with the Dissociation Kinetics of Radiolabeled Ligands. In the accompanying manuscript (Dunn & Raftery, 1997), the kinetics of dissociation of [^{3}H]AcCh, much more so than those of [^{3}H]SdCh, were accelerated when dissociation was initiated by dilution into buffer containing micromolar concentrations of unlabeled agonists. This led us to propose a model in which AcCh can transiently occupy an additional binding site (B), leading to a conformational change that reduces the affinity for [^{3}H]AcCh initially occupying site A. The much larger bis-quaternary SdCh is suggested to bridge the two subsites, and thus its dissociation is much less affected by the presence of unlabeled ligands.

In the IAS-monitored association kinetics, a second molecule of AcCh, but not SdCh, was observed to bind to the receptor. This raised the possibility that the binding of the second ligand, i.e., R*L → R^*L_2 reflects the binding to putative site B. In the association kinetics, as in the dissociation kinetics, if SdCh can bridge sites A and B, the binding of a second ligand would be prevented. In order to further investigate this possibility, it was first necessary to re-evaluate the AcCh binding kinetics in light of more recent findings.

Kinetics of Binding of AcCh to Its High-Affinity Sites Revealed by IAS Fluorescence. As noted above, Figure 4B was previously found to be consistent with the observed kinetics of Carb or AcCh binding to IAS-labeled AcChR (Dunn et al., 1980; Blanchard et al., 1982). Three phases are observed in the association kinetics, a fast phase ($k_{app} = 1-10$ s^{-1}), an intermediate phase ($k_{app} = 0.3-2$ s^{-1}) and a slow phase ($k_{app} = 0.03-0.12$ s^{-1}). Figure 5 shows the concentration dependencies of these phases and the curves (solid lines) which were calculated using the best fit parameters (Table 1) obtained from model fitting by Figure 4B. According to this model, the fast, intermediate, and slow phases may be correlated with isomerizations 2, 5, and 3, respectively. At low ligand concentrations, the reaction proceeds by the slow pathway toward C_1 and this correlates with the high-affinity binding observed in equilibrium binding experiments. According to Figure 4B and assuming

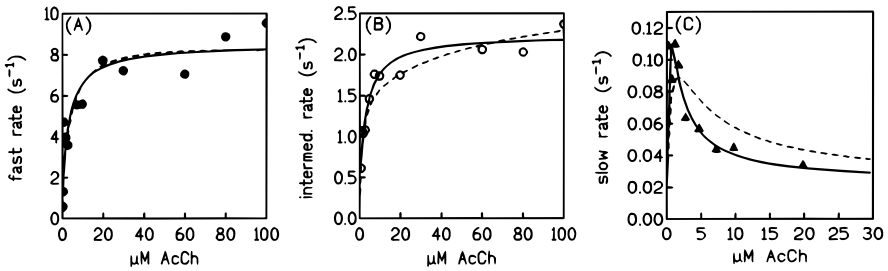

FIGURE 5: Analysis of kinetic data for AcCh binding to IAS-labeled *Torpedo* membranes according to Figure 4B (solid lines) or Figure 4C (dashed lines). The equations used for fitting Figure 4B were as described previously (Dunn et al., 1980):

$$k_{\text{fast}} = \frac{k_2[L]}{K_1 + [L]} + \frac{k_{-2}K_4}{K_4 + [L]}$$

$$k_{\text{inter}} = \frac{k_5[L^2]}{K_1K_2K_4 + K_4[L] + [L^2]} + k_{-5}$$

$$k_{\text{slow}} = \frac{k_3[L]}{K_1K_2 + [L] + [L^2]/K_4K_5} + k_{-3}$$

Equations describing Figure 4C were derived as previously described (Quast et al., 1979; Dunn et al., 1980), assuming that C_2 and R**L_2 rapidly equilibrate. The equation describing the fast phase remains as above, but k_{inter} and k_{slow} become

$$k_{\text{inter}} = \frac{k_5[L^2](1 + K_7/[L])}{K_1K_2K_4 + K_4[L] + [L^2]} + k_{-5}$$

$$k_{\text{slow}} = \frac{k_3[L]}{K_1K_2 + [L](1 + K_7/K_4K_5) + [L^2]/K_4K_5} + k_{-3}$$

Values of the parameters obtained by model fitting are given in Table 1. Nonlinear regression techniques, without constraint, were first used to fit the above equations to the rates of each phase. For Figure 4B, there was a high degree of consistency in the best fit parameters obtained for each phase and multiparameter fitting to all phases rapidly converged on a consistent set of parameters [see also Dunn et al. (1980)]. Fitting of Figure 4C required initial constraints (on K_7, k_{-3}, and k_{-5}), based on additional experimental evidence. These constraints are described in the text.

that the concentrations of di-liganded receptor are zero under these conditions, the equilibrium constant for high-affinity binding is the same as for Figure 4A, i.e.,

$$K_d = \frac{K_1K_2K_3}{1 + K_3(1 + K_2)}$$

Using the best fit parameters in Table 1, the estimated K_d of 30 nM is in reasonable agreement with equilibrium results (see above). At higher ligand concentrations, the predominant pathway is toward C_2 due to the binding of a second ligand with lower affinity. The binding of the second ligand occurs with an effective K_d, which may be approximated by K_4K_5/K_3 [see Quast et al. (1979)], of 12.9 μM. The values in Table 1 are in reasonable agreement with those previously reported for AcCh binding (Blanchard et al., 1982).

Discrepancies of Experimental Data from Predictions of Figure 4B. A prediction of Figure 4B is that, at high ligand concentrations, C_2, with two ligand molecules bound (or four if one considers the intact receptor, see above) will be the major species at equilibrium. Using the best fit parameters (Table 1), the total concentration of mono-liganded receptor (B_1 = RL + R*L + C_1), di-liganded receptor (B_2 = R*L_2 + C_2), and total bound ligand ($B_1 + 2B_2$) at equilibrium may be estimated according to Figure 4B. Figure 6A illustrates such a simulation using an AcChR concentration of 0.6 μM in high-affinity sites and an AcCh concentration of 1−20 μM. Over this concentration range the amount of di-liganded receptor becomes increasingly significant, and the total bound ligand becomes much greater than 0.6 μM. However, in the accompanying manuscript [Figure 4A of Dunn and Raftery (1997)] it was shown that, at these concentrations, the amount of bound [^{3}H]AcCh did not significantly exceed the number of high-affinity sites (as estimated by [^{125}I]-α-BuTx binding). It must, therefore, be concluded that, at AcCh concentrations below 20 μM, the amount of di-liganded receptor existing at equilibrium is insignificant, i.e., that Figure 4B is not a full description of the binding characteristics.

An additional discrepancy is that Figure 4B cannot account for the observed dissociation kinetics (accompanying manuscript). Since C_1 and C_2 are considered not to interconvert, this mechanism cannot explain the ability of unlabeled ligand to bind to the high-affinity receptor−[^{3}H]AcCh complex (represented by C_1 in Figure 4B) to accelerate the dissociation of the labeled ligand.

A Revised Mechanism To Describe the Kinetics of AcCh Binding to IAS-Labeled Membranes. A revised model that is generally consistent with the observed kinetics is depicted in Figure 4C. In this model, as previously considered for Figure 4B, it is assumed that the binding reactions (steps 1, 4, and 7) occur rapidly and that the fast, intermediate and slow phases in the observed kinetics arise from steps 2, 5, and 3, respectively. As before, the slow pathway toward C_1 dominates at low ligand concentrations, but at higher ligand concentrations, an additional ligand binds to R*L. For the purposes of discussion below, it is suggested that the binding of the first ligand is to site A (i.e., site A is occupied

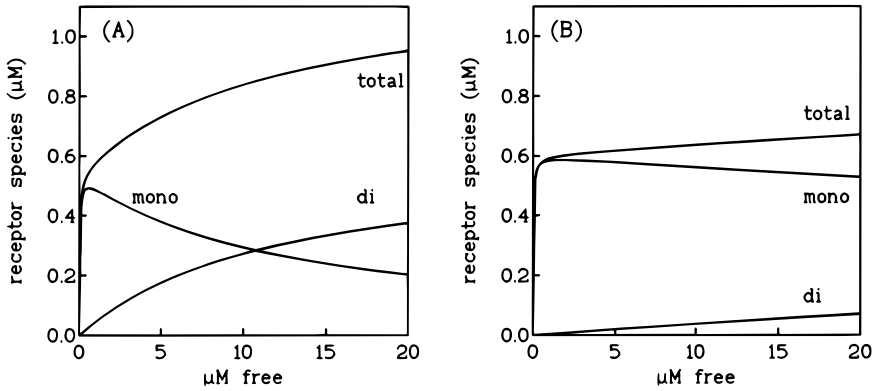

FIGURE 6: Simulations of the amount of bound AcCh according to Figure 4B and 4C. Figures show the estimated amount of total ligand bound, mono-liganded receptor ($RL+C_1$ in Figure 4B, $RL+C_1+C_2$ in Figure 4C), and di-liganded receptor ($R^*L_2 + C_2$ in Figure 4B, $R^*L_2+R^{**}L_2$ in Figure 4C). Data were calculated as below using the parameters listed in Table 1, assuming an initial receptor concentration ($[R_0]$) of 0.6 μM in high-affinity binding sites:

$$[\text{mono-liganded}] = \{[R_0](1 + 1/K_2 + 1/K_2K_3 + 1/K_2K_3K_6)\}/\{1 + K_1/[L] + 1/K_2 + 1/K_2K_3 + [L]/K_2K_4 + [L]/K_2K_4K_5 + 1/K_2K_3K_6\}$$

$$[\text{di-liganded}] = \{[R_0]([L]/K_2K_4 + [L]/K_2K_4K_5)\}/\{1 + K_1/[L] + 1/K_2 + 1/K_2K_3 + [L]/K_2K_4 + [L]/K_2K_4K_5 + 1/K_2K_3K_6\}$$

Note that, in the case of Figure 4B, $K_6 \rightarrow \infty$.

in C_1) and the binding of the second ligand is to site B. As noted above, the unusual concentration dependence of the slow phase requires that a second ligand can bind. However, in order to explain the apparent absence of di-liganded receptor at equilibrium (at concentrations up to 20 μM) it is now suggested that, although the pathway via R^*L_2 dominates the kinetics at higher concentrations, one of the two bound ligands again dissociates (step 7) in the formation of the final equilibrium *mono-liganded* complexes (C_1 and C_2). It is convenient to suggest that it is the site B ligand that dissociates in step 7, but this is not necessarily the case. Step 6 (i.e., the $C_1 \leftrightarrow C_2$ transition) is included to be at least qualitatively consistent with the observed dissociation kinetics. When dissociation is triggered by dilution alone, the pathway proceeds from C_1 (or C_2) to R*L via rate-limiting step k_{-3}, which in the accompanying manuscript is shown to be 0.023 s^{-1}. When dissociation is induced by dilution into buffer containing additional ligand, this can bind to C_2 (step 7) and dissociation via the $R^{**}L_2 \rightarrow R^*L_2$ pathway proceeds with rate limiting step k_{-5} (0.15 s^{-1}, see accompanying manuscript).

Best fit parameters for this model are listed in Table 1 and are shown in the dashed lines in Figure 5. One of the requirements considered in the model fitting was that the amount of di-liganded receptor existing at equilibrium is low. Fitting was, therefore, initially constrained using a value for K_7 of 40 μM. In addition, k_{-3} and k_{-5} were fixed by the limiting rates measured in studies of the dissociation kinetics. Although step 6 is not directly measured and there is no observed signal change that can be ascribed to this step, a value for K_6 can be estimated from the equilibrium requirement that $K_3K_6 = K_4K_5/K_7$ and the calculated value of 2.8 (Table 1) suggests that this equilibrium favors C_1. Furthermore, since neither k_6 nor k_{-6} appears to be rate-limiting in the dissociation kinetics, k_6 can be predicted to be ≥ 0.15 s^{-1}. According to Figure 4C, assuming that the concentrations of di-liganded species are zero, the apparent dissociation constant for high-affinity binding is given by

$$K_d = \frac{K_1K_2K_3K_6}{K_2K_3K_6 + K_3K_6 + K_6 + 1}$$

Using the parameters listed in Table 1, the estimated K_d is 21 nM, in good agreement with equilibrium results (see above).

While this model does not describe the IAS fluorescence data as well as the original Figure 4B, particularly in the slow phase fit (Figure 5C), it adequately describes the overall features of the observed kinetics. In addition, given the constraints that were imposed in the model fitting, the simulated amount of di-liganded receptor and total ligand bound at concentrations up to 20 μM (Figure 6B), are within 10% of experimentally determined values. The constraints that were introduced were necessitated by independent experimental observations. As discussed below, many other mechanisms were evaluated but none was found to provide better fits to the data. It should be emphasized that Figure 4C is unlikely to represent a complete description of the AcCh binding kinetics, mainly because of the very strict requirements imposed by the observed kinetic behavior of the slow phase, which does not conform to any simple mechanism [see Quast et al. (1979) and Dunn et al. (1980)]. A more complete description is difficult since some of the kinetic parameters are highly correlated and, especially at low ligand concentrations, the rate constants are sometimes quite close in magnitude. Also a complete description would require additional information on the mute steps in this model, especially steps 6 and 7. At the present time, however, Figure 4C is a useful working model to explain the differences in association and dissociation kinetics between AcCh and SdCh.

Binding of Other Bis-Quaternary Agonists to IAS-Labeled nAcChR. If the above model is correct, i.e., that SdCh can cross-link subsites A and B, then this places physical limits on the distance between these subsites. To further investigate this inter-site distance, we have synthesized a series of bis-quaternary SdCh analogues of varying length:

$$(CH_3)_3N^+CH_2CH_2OCO\text{-}(CH_2)_n\text{-}COOCH_2CH_2N^+(CH_3)_3$$

where $n = 0-10$. In preliminary experiments analogues in which $n = 0-6$ (C2−C8) have been shown to be agonists of the *Torpedo* receptor (H. Kawai and M. A. Raftery,

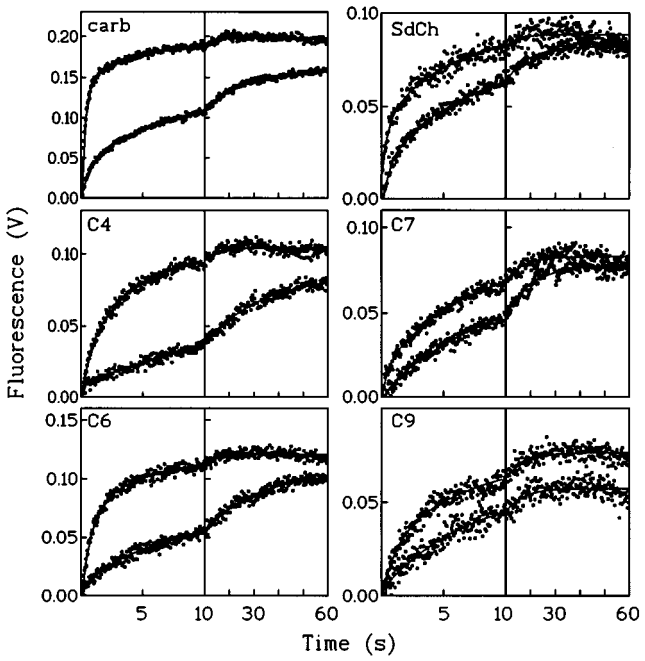

FIGURE 7: Representative kinetic traces of the binding of Carb, SdCh and bis-quaternary SdCh analogues (with varying chain length) to IAS-labeled nAcChR. The bis-quaternary ligands had the structure $(CH_3)_3N^+CH_2CH_2OCO(CH_2)_nCOOCH_2CH_2N^+(CH_3)_3$. In the figure, the ligands have been named according to the number of carbons between the ester groups, i.e., in C4, $n = 2$; in C9, $n = 7$, etc. According to this nomenclature, SdCh corresponds to C8 ($n = 6$). Stopped-flow data were recorded using a split time base as in Figure 2 for higher resolution of biphasic kinetics and these are shown on different scales to better illustrate the kinetics. Data shown are representative of recordings at two different ligand concentrations, with the lower trace being the lower concentration in each case. Concentrations used were 3 and 30 μM (Carb), 10 and 100 μM (C4), 3 and 100 μM (C6), 3 and 10 μM (SdCh), 1 and 10 μM (C7), and 1 and 10 μM (C9). For each ligand, these concentrations were selected to best illustrate the general appearance of the binding kinetics. The left hand side of the figure show ligands that are clearly Carb-like in their kinetics, i.e., an obvious slow phase at low concentrations that disappears at the expense of a much faster phase at higher concentrations. The ligands illustrated on the right are much more SdCh-like in their kinetics, i.e., biphasic time courses, with both phases becoming slightly faster at higher concentrations. As described in the text, ligands C2−C6 are Carb-like in their kinetic behavior and ligands C7−C12 are similar to SdCh.

unpublished observations). As described above, the binding of small mono-quaternary agonists such as Carb and of SdCh ($n = 6$) to IAS-labeled membranes display association kinetics that are obviously different (see Figure 7 for comparison). The kinetics of binding of the above series of compounds to IAS labeled membranes have been studied to determine at what point in the series the kinetics change from Carb-like to SdCh-like. Representative kinetic data are shown in Figure 7. Ligands C2 ($n = 0$) to C6 ($n = 4$) were clearly Carb-like in their kinetics but C7 and larger analogues ($n = 5-10$) behaved similarly to SdCh. Thus ligands with $n \geq 5$ appear to be large enough to either physically cross-link the subsites, or at least sterically inhibit the binding of the second ligand.

DISCUSSION

The results reported above suggest that the mechanism of high-affinity binding of AcCh to nAcChR, as monitored by changes in IAS fluorescence, is more complex than previously reported (Dunn et al., 1980; Blanchard et al., 1982; Dunn & Raftery, 1993). In order to explain complexities in the association kinetics, and also in the dissociation kinetics (accompanying manuscript), a model is proposed in which each high-affinity site is made up of two subsites. Although both sites *can* be simultaneously occupied, the major species at equilibrium is the mono-liganded state. The notion of receptor binding sites being formed by multiple subsites is not new. In 1979, De Lean et al. proposed a general multi-subsite model to explain the often complex pharmacological properties observed when flexible ligands bind to their receptors. More recently, this model has been developed further to show that ligand-induced accelerated dissociation, which is observed in many receptor systems [see Prinz and Striessnig (1993)], can be expected if ligands compete for multiple attachment points within the binding site (Rothman et al., 1991; Prinz & Striessnig, 1993). In these previous reports, as suggested here, it is proposed that there are transient states in which more than one ligand can occupy a binding site. Mechanistically, it is not possible to distinguish between two ligands competing for different attachment points within one site, or competing for separate binding sites which are mutually exclusive at equilibrium. In the present study, we have therefore also investigated the binding of SdCh and other bis-quaternary ligands, in an attempt to provide some structural basis for correlation with the observed kinetics of binding. The kinetics of SdCh binding to IAS-labeled receptor preparations could be described by a mechanism in which two conformational changes follow the formation of the initial complex (Figure 4A). In an early study in which SdCh binding was monitored by changes in protein intrinsic fluorescence (Barrantes, 1978), a similar mechanism, although without the slower transition, was proposed. The major difference in the SdCh kinetics from those of other ligands such as Carb (Dunn et al., 1980) or AcCh (Blanchard et al., 1982) is the absence of a second pathway involving the binding of an additional ligand. Similarly, the dissociation kinetics (accompanying manuscript) are simpler than those of AcCh since, for SdCh, it is not necessary to invoke the binding of additional ligand. Although other interpretations are possible, the simplest suggestion is that SdCh is sufficiently large to bridge the two subsites, or at least sterically inhibit the binding of the second ligand. Examination of a series of bis-quaternary ligands suggests that the binding of a second ligand can occur for ligands C6 and shorter, while C7−C12 act like SdCh (C8). This represents a first step toward physically mapping the receptor sites.

A revised mechanism (Figure 4C) is proposed to account for the kinetics of AcCh binding. According to this mechanism, although two AcCh molecules can transiently occupy the binding site(s), one ligand again dissociates during the approach to equilibrium. Although one can only speculate about the physiological significance of such a mechanism, one consequence is that at higher AcCh concentration, the equilibrium state is reached more quickly via the $R^*L_2 \rightarrow C_2$ pathway. Since the observed conformational transitions are likely to represent desensitization mechanisms [see Dunn and Raftery, (1993)], this is consistent with electrophysiological studies of nAcChRs which have shown that desensitization occurs more rapidly at higher AcCh concentration (Adams, 1981).

While Figure 4C is generally consistent with the observed kinetics, it is not a complete description and there remain some quantitative anomalies that cannot presently be addressed. In order to reduce the amount of di-liganded receptor present at equilibrium, fitting procedures were constrained using a value of 40 μM for K_7. Without this constraint, a much better fit can be obtained but the best fit value for K_7 is only 1−2 μM. This latter value is in excellent agreement with the dissociation kinetics, where the EC_{50} for the acceleration of dissociation of [^{3}H]AcCh by AcCh, suggested to be due to the binding of unlabeled ligand to the equilibrium C_2 complex (see above) was 2 μM (accompanying manuscript). This, however, would mean that additional bound ligand should be readily detectable in equilibrium binding studies. Thus the true binding mechanism is likely to be more complex than the already complex model depicted in Figure 4C. Other modifications of Figure 4B have been evaluated but these have been shown to be less compatible with the experimental observations. If, for example, the second ligand is allowed to dissociate in step 5 during the $R^{**}L_2 \rightarrow C_2$ transition, then the intermediate rate becomes very large at high ligand concentration, due to the ligand-dependence of the reverse rate constant which becomes $k_{-5}[L]$. A two-state model in which a ligand binding step occurs in the $C_1 \leftrightarrow C_2$ transition is incompatible with the observed kinetics since it predicts a single exponential process (Janin, 1973). Although a number of investigators, using other approaches, have found variations of two-state models to be consistent with their data [see Prinz and Maelicke (1993)], as discussed previously [see Quast et al. (1979) and Dunn et al. (1980)], such mechanisms do not adequately describe the kinetics observed using IAS fluorescence.

In conclusion, in this and the companion article, it is shown that the two nicotinic receptor agonists, AcCh and SdCh display differences in their association and dissociation kinetics. These differences can be explained if, for each high-affinity agonist binding site, there are two subsites for AcCh which can both be occupied by a single SdCh molecule. These observations, in addition to the likely existence of distinct low-affinity agonist sites [see Dunn and Raftery (1993)], further demonstrate the complexity of the nAcChR in terms of its binding sites. As noted in the introduction, despite the wealth of information that has been accumulated about the structure and function of this receptor, many of its mechanisms of action remain to be clarified.

ACKNOWLEDGMENT

The authors thank Rick Thuynsma (Alberta) and David Okita (Minnesota) for expert technical assistance. We are also grateful to Mark Arriola for synthesis of the SdCh analogues used in this work.

REFERENCES

Adams, P. R. (1981) *J. Membr. Biol. 58*, 161−174.
Barnard, E. A. (1992) *Trends Biochem. Sci. 17*, 368−374.
Barrantes, F. J. (1978) *J. Mol. Biol. 124*, 1−26.
Betz, H. (1990) *Trends Neurosci. 14*, 458−461.
Blanchard, S. G., Dunn, S. M. J., & Raftery, M. A. (1982) *Biochemistry 21*, 6258−6264.
Blount, P., & Merlie, J. P. (1989) *Neuron 3*, 349−357.
Boyd, N. D., & Cohen, J. B. (1980) *Biochemistry 19*, 5353−5358.
Changeux, J.-P. (1995) *Biochem. Soc. Trans. 23*, 195−205.
Changeux, J.-P., Devillers-Thiéry, A., & Chemouilli, P. (1984) *Science 225*, 1335−1345.
Changeux, J.-P., Galzi, J.-L., Devillers-Thiéry, A., & Bertrand, D. (1992) *Q. Rev. Biophys. 25*, *395*−432.
Czajkowski, C., Kaufmann, C., & Karlin, A. (1993) *Proc. Natl. Acad. Sci. U.S.A. 90*, 6285−6289.
Damle, V. N., & Karlin, A. (1978) *Biochemistry 19*, 3924−3932.
De Lean, A., Munson, P. J., & Rodbard, D. (1979) *Mol. Pharmacol. 15*, 60−70.
Dunn, S. M. J., & Raftery, M. A. (1982a) *Proc. Natl. Acad. Sci. U.S.A. 79*, 6757−6761.
Dunn, S. M. J., & Raftery, M. A. (1982b) *Biochemistry 24*, 6264−6272.
Dunn, S. M. J., & Raftery, M. A. (1993) *Biochemistry 32*, 8608−8615.
Dunn, S. M. J., & Raftery, M. A. (1997) *Biochemistry 36*, 3846−3853.
Dunn, S. M. J., Blanchard, S. G., & Raftery, M. A. (1980) *Biochemistry 19*, 5645−5652.
Dunn, S. M. J., Conti-Tronconi, B. M., & Raftery, M. A. (1983) *Biochemistry 22*, 2512−2518.
Dunn, S. M. J., Conti-Tronconi, B. M., & Raftery, M. A. (1993) *Biochemistry 32*, 8616−8621.
Dunn, S. M. J., Bateson, A. N., & Martin, I. L. (1994) *Int. Rev. Neurobiol. 36*, 51−96.
Galzi, J. L., Bertrand, D., Devillers-Thiéry, A., Revah, F., Bertrand, S., & Changeux, J.-P. (1991) *FEBS Lett. 294*, 198−202.
Grünhagen, H.-H., Iwatsubo, M., & Changeux, J.-P. (1977) *Eur. J. Biochem. 80*, 225−242.
Haugland, R. P. (1970) Ph.D. Dissertation, Stanford University.
Heidmann, T., & Changeux, J.-P. (1979) *Eur. J. Biochem. 94*, 255−279.
Heidmann, T., & Changeux, J.-P. (1980) *Biochem. Biophys. Res. Commun. 97*, 889−896.
Hollenberg, M. D. (1991) *FASEB J. 5*, 178−186.
Holmstedt, B., & Whittaker, V. P. (1958) *Br. J. Pharmacol. 13*, 308−315.
Janin, J. (1973) *Prog. Biophys. Mol. Biol. 27*, 77−120.
Kao, P. N., & Karlin, A. (1986) *J. Biol. Chem. 261*, 8085−8088.
Kao, P. N., Dwork, A. J., Kaldany, R.-R., Silver, M. L., Wideman, J., Stein, S., & Karlin, A. (1984) *J. Biol. Chem. 259*, 11662−11665.
Karlin, A., & Akabas, M. H. (1995) *Neuron 15*, 1231−1244.
Kellaris, K. V., & Ware, D. K. (1989) *Biochemistry 28*, 3469−3482.
Kreienkamp, H.-J., Utkin, Y. N., Weiese, C., Machold, J., Tsetlin, V. I., & Hucho, F. (1992) *Biochemistry 31*, 8239−8244.
Mecklenborg, K. T., & Orchin, M. (1958) *J. Org. Chem. 23*, 2023−2030.
Middleton, R. E., & Cohen, J. B. (1991) *Biochemistry 30*, 6987−6997.
Moore, H.-P. H., & Raftery, M. A. (1979) *Biochemistry 18*, 1862−1867.
Moskovitz, R., & Gershoni, J. M. (1988) *J. Biol. Chem. 263*, 1017−1022.
Noda, M., Takahashi, H., Tanabe, T., Toyosato, M., Kikyotani, S., Furutani, Y., Hirose, T., Takashima, H., Inayama, S., Miyata, T., & Numa, S. (1983) *Nature 302*, 528−532.
Ochoa, E. L. M., Chattopadhyay, A., & McNamee, M. G. (1989) *Cell Mol. Neurobiol. 9*, 141−178.
O'Leary, M. E., & White, M. M. (1992) *J. Biol. Chem. 267*, 8360−8365.
Pederson, S. E., & Cohen, J. B. (1990) *Proc. Natl. Acad. Sci. U.S.A. 87*, 2785−2789.
Prinz, H. (1988) *Neurochem. Int. 12*, 109−119.
Prinz, H., & Maelicke, A. (1983) *J. Biol. Chem. 258*, 10273−10282.
Prinz, H., & Maelicke, A. (1992) *Biochemistry 31*, 6728−6738.
Prinz, H., & Striessnig, J. (1993) *J. Biol. Chem. 268*, 18580−18585.
Quast, U., Schimerlik, M. I., & Raftery, M. A. (1979) *Biochemistry 18*, 1891−1901.
Raftery, M. A., Hunkapillar, M. W., Strader, C. D., & Hood, L. E. (1980) *Science 208*, 1454−1457.
Rothman, R. B., Reid, A., Mahboubi, A., Kim, C.-H., deCosta, B. R., Jacobson, A. E., & Rice, K. C. (1991) *Mol. Pharmacol. 39*, 222−232.

Sekull, A. A., & Holland, W. C. (1961) *J. Pharm. Exp. Ther. 132*, 171−175.
Sekull, A. A., & Holland, W. C. (1963) *Arch. Int. Pharmacodyn. 146*, 93−98.
Sieghart, W. (1995) *Pharmacol. Rev. 47*, 181−234.
Sine, S. M. (1993) *Proc. Natl. Acad. Sci. U.S.A. 90*, 9436−9440.
Sine, S. M., & Claudio, T. (1991) *J. Biol. Chem. 266*, 19369−19377.
Sine, S. M., Kreienkamp, H.-J., Bren, N., Maeda, R., & Taylor, P. (1995) *Neuron 15*, 205−211.
Stroud, R. M., McCarthy, M. P., & Shuster, M. (1990) *Biochemistry 29*, 11009−11023.
Taylor, P., Brown, R. D., & Johnson, D. A. (1983) *Curr. Top. Membr. Transp. 18*, 407−444.
Tomaselli, G. F., McLaughlin, J. T., Jurman, M. E., Hawrot, E., & Yellen, G. (1991) *Biophys. J. 60*, 721−727.
Wolosin, J. M., Lyddiatt, A., Dolly, J. O., & Barnard, E. A. (1980) *Eur. J. Biochem. 109*, 494−505.

BI9615046